A 4 V Cathode Compatible, Superionic Conductive Solid Polymer Electrolyte for Solid Lithium Metal Batteries with Long Cycle Life

*Wenfeng Liang, Yunfan Shao, Yu-Ming Chen, Yu Zhu**

Department of Polymer Science,

University of Akron

170 University Circle, Akron, Ohio 44325, United States

*Address correspondence to: Yu Zhu (yu.zhu@uakron.edu)

KEYWORDS: Polymer Electrolyte, Phase Diagram, Superionic Conductivity, Lithium Metal Battery, 4 V Cathode

ABSTRACT: A highly conductive and electrochemically stable dual-salt solid polymer electrolyte (SPE) for high capacity cathode was developed. A phase-diagram approach was adopted to provide rational guidance for achieving a high ionic conductivity (over 1.76 mS/cm at 30 ºC). The synergy of combining different salts rendered the SPE a superior electrochemical stability with an electrochemical window from 0 to 5 V (*vs*. Li^+/Li) in linear sweep voltammetry and up to 4.15 V in lithium metal batteries (LMBs). The SPE exhibited outstanding long-term stability performance in lithium plating/striping experiments under current densities from 0.08 to 0.5 mA/cm^2. The solid-state lithium metal batteries (with $LiNi_{0.8}Co_{0.15}Al_{0.05}O_2$, NCA, cathode) exhibited initial capacities of 165 mAh/g at 0.1 C rate and 113 mAh/g at 1 C rate at 30 ºC. The average Coulombic efficiency of solid-state batteries was over 99.99% in the first 1000 cycles at

1 C rate and the capacity retention was 66% after 1000 cycles. In addition, the per cycle capacity fading after the initial 100 cycles was only 0.017 %/cycle. The results demonstrate that the SPE is a promising candidate electrolyte for high energy density solid-state lithium metal battery.

1. INTRODUCTION

Since the commercialization of lithium ion battery (LIB) in 1990s,[1] the rechargeable lithium batteries became the most attractive battery technology, used widely in portable electronics and recently being implemented in electrical vehicles and large scale grid-energy storage systems.[2–6] However, the low power and energy density of current LIB electrodes and potential safety concerns of the flammable organic solvent based electrolytes hinder the further utilization of LIB in many emerging applications.[7,8] Extensive research has been conducted to develop superior alternative electrode materials to improve the energy density of the LIB.[9–12] Among those new materials, lithium metal anode is the holy grail for future lithium batteries due to the high theoretical specific capacity (3,860 mAh/g), the low redox potential (-3.04 V *vs*. standard hydrogen electrode) and the low mass density (0.56 g/cm^3).[13] However, despite substantial efforts on developing lithium metal batteries (LMBs), its practical applications remained stagnant due to several challenges: First, the flammable organic liquid electrolyte is a potential safety issue, which would be particularly severe with the failure of a lithium metal anode based battery. Second, the uneven lithium plating/stripping process on the lithium metal electrode would result in uncontrollable dendritic growth, which may penetrate the separator and cause internal short circuit, leading to battery thermal runaway.[14–16] Finally, the unstable solid electrolyte interphase formation on the lithium metal anode could continuously consume the electrolyte and lithium source in the battery, resulting

in a decrease in Coulombic efficiency and an increase in cell impedance.[17,18] As such, the implementation of lithium metal anode in current lithium ion batteries to replace the graphite anode is essential to enhance energy density but challenging. In addition, the successful implementation of lithium metal anode also serves as a basis for many beyond lithium ion battery techniques such as lithium- sulfur battery and lithium-oxygen battery.[19,20]

The implementation of lithium metal anode require nonflammable, dendrite mitigation and electrochemically stable electrolyte. One straight forward way is to use solid electrolyte with strong shear modulus, where the lithium dendrite formation could be mitigated and even completely suppressed.[21] In order to achieve comparable performance in the battery, it is necessary to design solid-state electrolyte with a high ionic conductivity and compatible with commercial cathodes. Solid polymer electrolytes (SPEs) emerged as a candidate for solid-state lithium metal battery due to their low cost and flexible nature. The most investigated polymer electrolyte, poly(ethylene oxide) (PEO) and alkali metal salt composite, was extensively studied since 1970s.[22,23] Other than PEO, many other polymers, for instance, poly(ethylenimine)(PEI),[24] poly(acrylonitrile)(PAN),[25] poly(vinylidene fluoride)(PVDF)[26] and poly(methyl methacrylate)(PMMA),[27] were also investigated. Up until now, PEO remained to be arguably the best polymer host due to its outstanding solvability with lithium salts and high efficiency in the coordination with lithium ions.[28,29] The drawback of the PEO is that it exhibits a low ionic conductivity at room temperature (~10^{-3} to 10^{-2} mS/cm) and shows relatively low lithium ion transference number (t_{Li+}) around 0.2-0.5.[30–32] While organic liquid plasticizers, such as ethylene carbonate (EC) and dimethyl carbonate (DMC), could be used to enhance the ionic conductivity

in PEO by decreasing its crystallinity, these small organic molecules adversely affect the physical properties of the SPE and decrease the thermal stability of SPE.[33] Previously, it was reported that plastic crystal materials, such as succinonitrile (SN), could effectively increase the ionic conductivity in PEO-based SPE system as an alternative solid plasticizer. Conductive SPE with added SN was demonstrated and showed good performance with acceptable mechanical strength.[34,35] However, most SPE systems were tested in lithium ion batteries with lithium iron phosphate (LFP) as the cathode due to the limited potential range of PEO electrolyte in the cell(< 4.0 V). Therefore, a SPE with wider electrochemical window that enables the utilization of more advanced 4 V cathodes such as $LiNi_{0.8}Co_{0.15}Al_{0.05}O_2$ (NCA), $LiNi_xCo_xMn_xO_2$ (NMC) and $LiCoO_2$ (LCO) is required.

Herein, a dual-salt based solid polymer electrolyte was developed. The SPE was prepared by mixing lithium bis(oxalate)borate (LiBOB) and lithium bis(trifluoromethanesulphonyl)imide salt (LiTFSI), together with solid plasticizer succinonitrile (SN) in poly(ethylene glycol) diacrylate (PEGDA). The free standing SPE film was prepared by crosslinking the SPE precursor through UV curing. Guided by a ternary phase diagram analysis, the composition of the dual-salt SPE with high ionic conductivity at 30 ºC was achieved. Thermal and electrochemical characterizations were carried out to determine the stability of the SPE. Lithium metal batteries with Li|SPE|NCA assembly were fabricated and tested. The results indicated that the dual-salt SPE performed outstanding stability with 4 V cathode.

2. RESULTS AND DISCUSSION

2.1 Synthesis of Solid Polymer Electrolyte

The most challenging task for developing SPE is to achieve high ionic conductivity. Two mechanisms have been developed to explain the Li^+ migration in the solid polymer matrix.[36] In the amorphous region of a polymer matrix, the lithium ions and counter anions dissociate and then the lithium ions could hop from one coordination site to another adjacent coordination site. Such a repetitively hopping and coordination with adjacent coordinate sites is driven by the motion of amorphous polymer chains.[37] While in the crystalline region of a polymer matrix, lithium ions move by hopping over spiral channels, which are created by the folding of crystalline polymer chains. In the PEO-based polymer electrolyte system, lithium ion migration is believed to occur by the formation and disruption of coordination bonds between lithium ions and ether groups. Therefore, the fast segmental relaxation will improve ionic conductivity.[38,39] Under this scenario, in order to achieve the optimized ionic conductivity, it is necessary to determine the amorphous region composition in the polymer electrolyte. For this purpose, a ternary phase diagram of crosslinked PEGDA/Lithium salt/Plasticizer was constructed with the assistance from polarized optical microscopy image characterization shown in Figure 1a. In this experiment, samples with different ratios of PEGDA, SN and lithium salts were prepared, then casted on a glass slide and then cured under UV light to form the SPE film. The phase diagram should be measured at different temperatures to simulate the broad operating temperatures of different battery applications. Following the general understanding of SPE, the amorphous region on phase diagram at the high temperature should be larger than that at the low temperature. The phase diagram of SPE at - 10 ^oC, 25 ^oC and 70 ^oC were studied. As shown in Figure 1a, at -10 ^oC, the large isotropic region,

represented by blue dots, can be identified in the triangular phase diagram. The amorphous region of the polymer matrix could be ascribed to the hindrance of crystallization by the crosslinked polymer network and plasticization effects of solid SN. The polarized optical microscopy image of amorphous composite region was completely dark, as shown in Figure 1b. The polymer crystallization region was observed when the concentration of PEGDA was nearly 100 %, represented by green dots. The clear crystal structure was found in the corresponding polarized microscopy image in Figure 1c. On the other hand, when the percentage of polymer content was low in the composites, the free-standing SPE membrane could not be formed even after crosslinking. Instead, the gel-like electrolyte was obtained (indicated by the orange dots.) In addition, a phase separation was observed when the concentrations of lithium salt or plasticizer (showing as purple and red dots, respectively) were high in the composite. Overall, based on the result of the ternary phase diagram of crosslinked PEGDA/Lithium salt/Plasticizer, the feasible working region was determined, represented by the blue shadow region in the triangular phase diagram. The ternary phase diagrams of composites at 25 ºC and 70 ºC were shown in the supporting information (Figure S1). It is clear that the amorphous regions at 25 ºC and 70 ºC were larger. However, the battery application requires a wide operating temperature range, thus an optimized composition was further investigated based on the ternary phase diagram at -10 ºC. Figure 1d-f show the photos of the deformability test of free-standing SPE membranes, prepared by photo-crosslinking of the ternary polymer precursor with the composition within the amorphous region. As illustrated in Fgiure1d-f, the transparent SPE membrane are flexible and twistable so

that it can be used as the ionic conducting film in battery fabrication to replace the liquid electrolyte and separator.

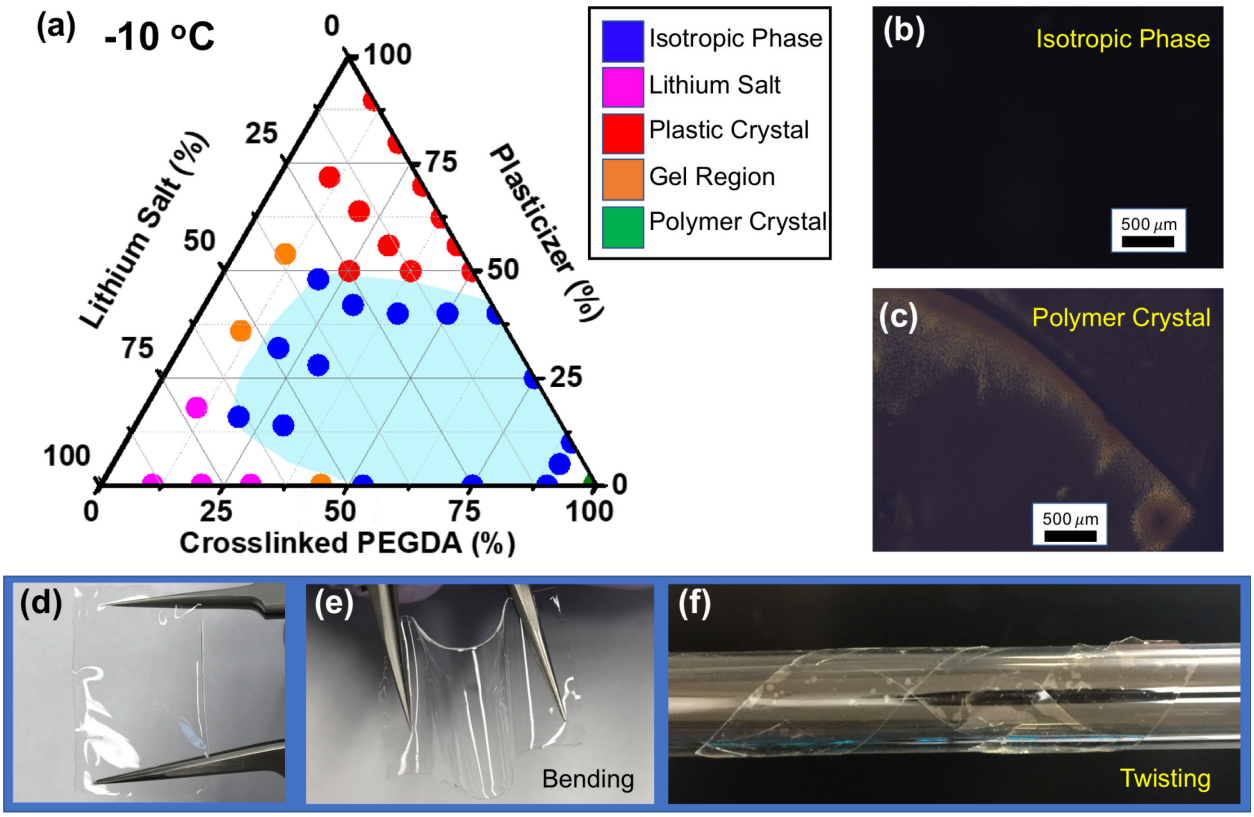

Figure 1. (a) Ternary phase diagram of crosslinked PEGDA/Lithium salts/Plasticizer at -10 ºC based on the polarized optical microscopy image characterization. Blue dots: isotropic phase; purple dots: lithium salt segregation; red dots: plastic crystal segregation; green dots: polymer PEGDA crystallization. The shadowed area, which is highlighted for clarity, indicates the isotropic phase range. (b) Polarized optical microscopy images corresponding to isotropic phase and (c) polymer PEGDA crystal. (d-f) The picture of flexible SPE film produced with composition in the amorphous region (crosslinked PEGDA:Plasticizer:Lithium salts = 25:40:35), demonstrating the bendability and twistability.

The ionic conductivity and lithium ion transference number are regarded as the two most important parameters for SPE. Based on the ternary phase diagram, the ionic conductivity of selected ratios from the amorphous region was measured at 30 ºC. And the conductivity gradient is plotted in the phase diagram, shown in Figure 2a. The optimized ionic conductivities were reached at the ratios of 20:50:30 (crosslinked PEGDA:Plasticizer:Lithium salts) and 25:40:35, where the average values are 0.76 mS/cm and 0.72 mS/cm, respectively. The highest ionic conductivity measured in an individual sample reached 1.76 mS/cm at 30 ºC. The SPEs with optimized compositions were used in the following experiments.

The temperature-dependent ionic conductivity for SPE (crosslinked PEGDA:Plasticizer:Lithium salts=25:40:35) was also investigated as shown in Figure 2b. With the increase of the temperature, the polymer chain mobility would increase, leading to higher ionic conductivity. The average ionic conductivity of the SPE is 0.72 mS/cm at 30 ºC. As the temperature was increased to 100 ºC, the ionic conductivity was increased to 4.77 mS/cm. The conductivity dropped to 0.091 mS/cm when the temperature was 0 ºC. The Vogel-Tammann-Fulcher model empirical formula was used to perform the curve fitting (as plotted in red line in Figure 2b).[40] The activation energy of SPE is 7.23 KJ/mol and other fitting results are shown in Table S1. The lithium ion transference number, t_{Li+}, was obtained by using the potentiostatic polarization method and electrochemical impedance measurement.[30,41,42] Figure S2 demonstrates the polarization curve and the AC impedances. Further details about the transference number calculation are shown in the supporting information. The calculated t_{Li+} is approximately 0.535,

which is higher than that of the conventional liquid electrolyte (usually less than 0.5), due to the entrapment of the large anions of LiTFSI by the polymer network.[43]

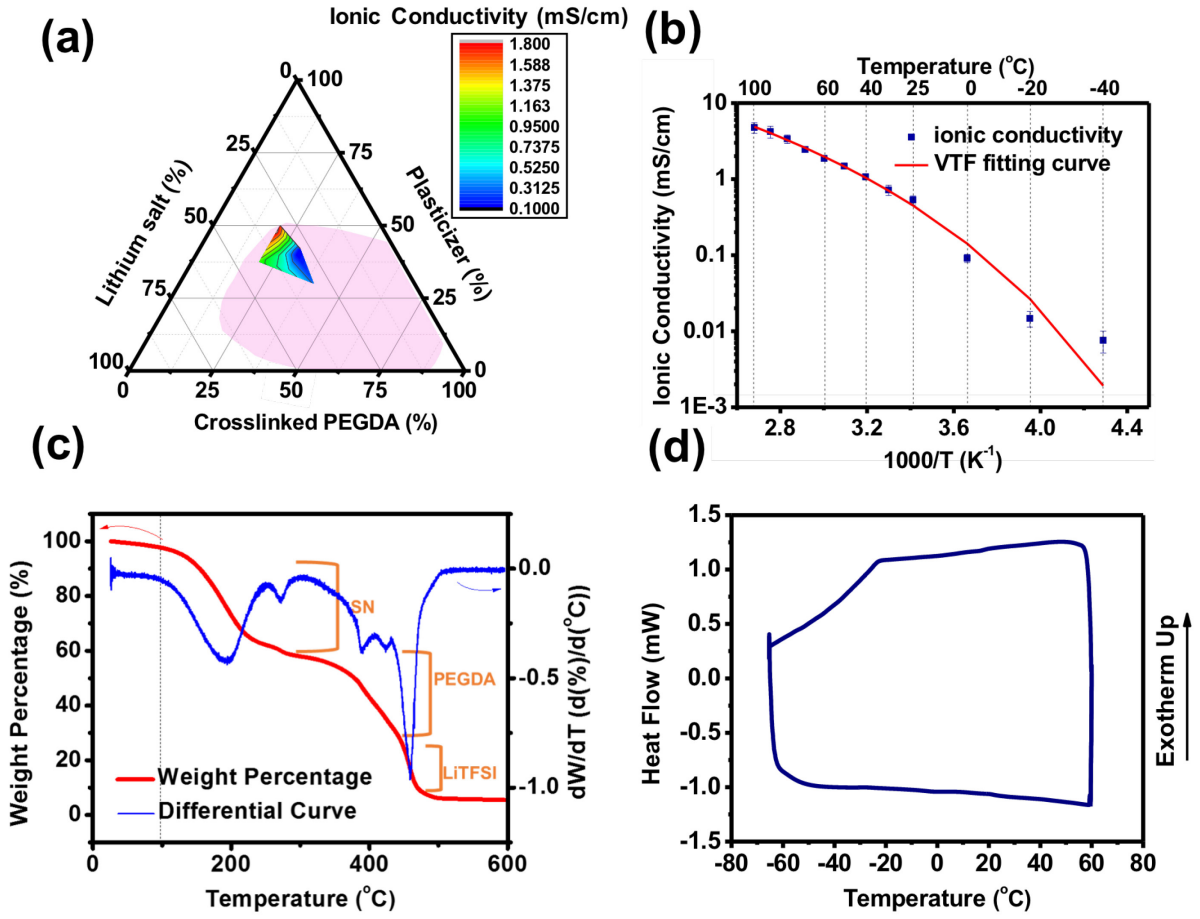

Figure 2. (a) The ionic conductivity (at 30 °C) of SPE on the ternary phase diagram. The shadowed region is the suggested isotropic phase region for the SPE film fabrication based on the phase diagram analysis data derived at -10 °C. The colored gradient area in the center represents the ionic conductivity of the SPE at 30 °C. (b) The temperature-dependent ionic conductivity of the SPE. (c) The TGA thermogram of the SPE. (d) The DSC thermogram of the SPE film.

The thermal properties of the SPE was evaluated by thermogravimetric analysis (TGA) and differential scanning calorimetry (DSC). As shown in TGA results (Figure 2c), the crosslinked

SPE is thermally stable over 100 ºC, pointed out by a dash line in the figure 2c. The weight loss of SPE matches well with the components ratio in the composite. The weight loss of the SPE were compared with gel electrolyte and liquid electrolyte in literature (Figure S8). The results indicate that the polymer electrolyte in this work performs like solid state electrolyte. Figure 2d shows the DSC results of the crosslinked SPE film. With the plasticizer, DSC curve shows flat line without obvious peaks, demonstrating an amorphous state of SPE.

2.2 Electrochemical Tests of Solid Polymer Electrolyte

For LMB with high potential cathodes (> 4 V vs. Li^+/Li), a large, stable electrochemical window is essential. Most reported SPE system used LiTFSI as lithium salt due to the high ion dissociation ratio. In this work, an additional salt, LiBOB was added to the SPE (with the molar ratio of LiTFSI:LiBOB=1:0.085) to improve the electrochemical stability. Previously, LiBOB was reported to improve electrochemical stability in the liquid electrolyte based battery.[44] It is therefore expected to achieve a higher electrochemical stability with additional LiBOB added in the SPE system. A recent exploration also indicated that the LiTFSI:LiBOB has synergetic effect for stabilizing LFP cathode based LMBs.[45] In this work, the mole ratio of LiTFSI:LiBOB is determined by the maximum solubility of LiBOB in the SPE system. Linear sweeping voltammetry (LSV) test was carried out to determine the electrochemical working potential range (Figure 3a). The dual-salt SPE exhibits a stable potential window up to 5.0 V *vs*. Li^+/Li. The CV result is shown in Figure 3b. The peaks between 0.4 V and -0.5 V (*vs*. Li^+/Li) correspond to the lithium plating and stripping processes. From CV results, the SPE is stable up to 4.8 V (*vs*. Li^+/Li) without showing any obvious oxidation peaks and remains unchanged in following several cycles.

As comparison, single salt (LiTFSI) SPE films were also prepared and tested in LSV and CV experiments. The results are shown in Figure S3. It confirmed that LiBOB could help stabilize the SPE and accommodate the serious deterioration at a higher potential range, and hence, improve the electrochemical compatibility with high potential cathodes.

To further investigate the electrochemical stability for Li metal anode in the SPE battery system, a symmetric Li|SPE|Li cell was fabricated and subsequently implemented for plating/striping tests. As shown in Figure 3c, the cell was tested at current density of 0.1 mA/cm^2 for a period of 1.5 h for each half cycle. During charge/discharge process, lithium ions were plated/stripped on the Li metal anode surface, which would increase the surface roughness and lead to the formation of dendrite. Figure 3c represents the time-dependent potential profile of the symmetric cell cycled over 2300 hours at 30 ºC. Figure 3d and 3e are the enlarged views of Figure 3c, showing the beginning and ending parts of the test, respectively. In Figure 3c, a slight increase in the overpotential at the beginning was observed, which could be ascribed to the SEI layer formation. Then in following cycles, the potential decreased and became increasingly stable. The plating/stripping experiments were also conducted at current densities of 0.5 mA/cm^2 (6 min per half cycle, 15 min per half cycle and 20 min per half cycle) and 0.08 mA/cm^2 (1.5 h per half cycle), shown in Figure S4. The cells showed stable potential profiles up to 1700 hours (0.5 mA/cm^2, 6 min per half cycle), 3000 hours (0.08 mA/cm^2, 1.5 h per half cycle) respectively. Even with extended stripping/plating time (15 min per half cycle and 20 min per half cycle at 0.5 mA/cm^2), the initial test indicated that the SPE could be cycled for more than 100 hours. All these results

exhibited an exceptional long-term cycling performance of the dual-salt SPE system with Li metal anode.

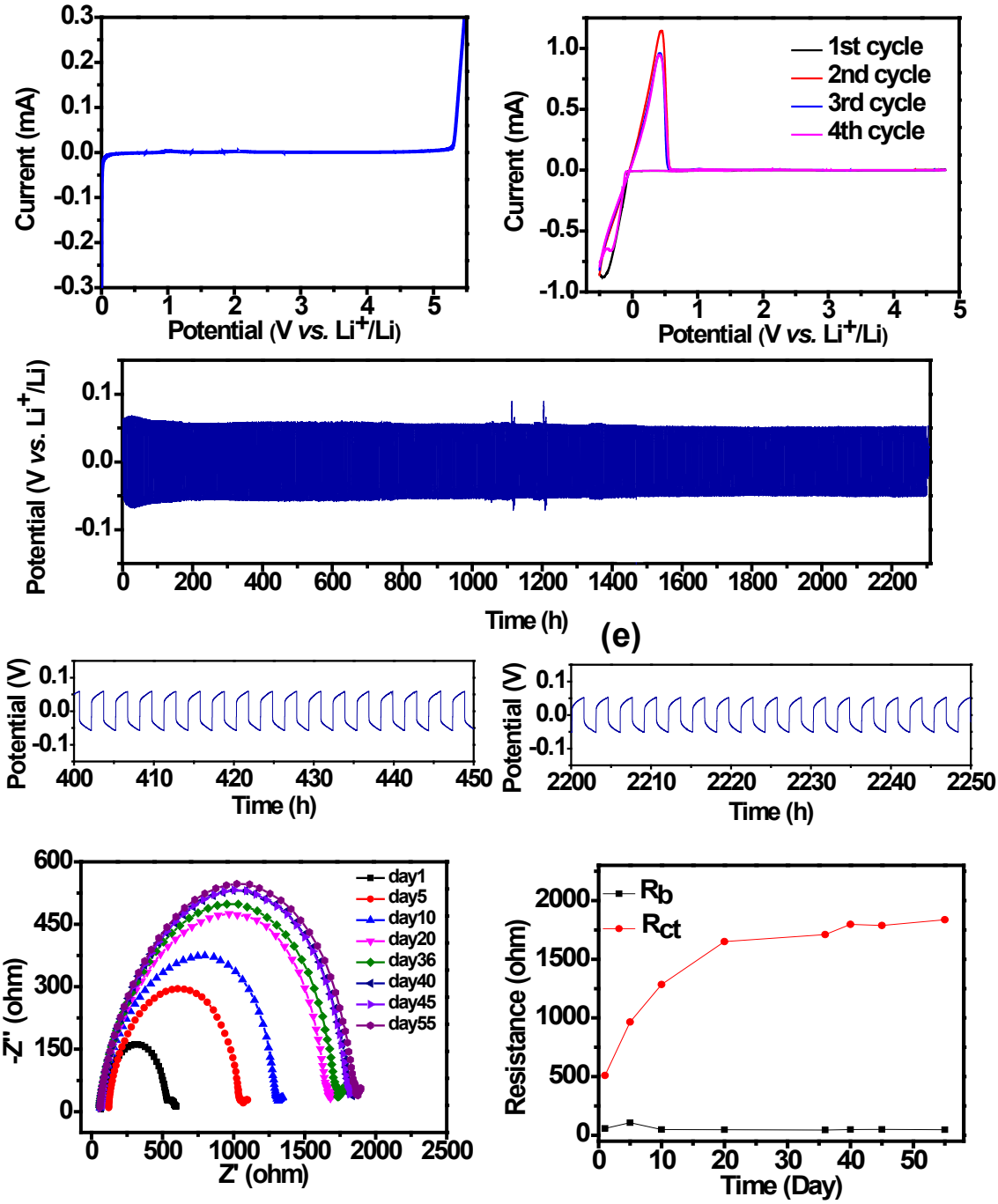

Figure 3. (a) LSV of the dual-salt (LiTFSI/LiBOB) SPE. (b) CV of the dual-salt (LiTFSI/LiBOB) SPE. (c-e) Lithium plating/stripping test conducted at a current density of 0.1 mA/cm^2. The charge

and discharge time were fixed at 1.5 hrs. (d) and (e) are the enlarged views of (c), showing the beginning and ending parts of the test, respectively. (f) Electrochemical impedance spectra of dual-salt (LiTFSI/LiBOB) as a function of storage time at 30 °C. Frequency range: 0.1 Hz – 0.1 MHz (g) The changes of bulk resistance (R_b) and charge transfer resistance (R_{ct}) over time (30 °C).

Since the stability of the dual-salt SPE/Li metal anode interface is an essential parameter for long-term stability of rechargeable lithium metal batteries, electrochemical impedance spectroscopy (EIS) was used to analyze the interfacial property. In this experiment, symmetric Li|SPE|Li cells were examined and EIS was measured over time under 30 °C (Figure 3f). Figure 3g reported the corresponding charge transfer resistance (R_{ct}) and bulk resistance (R_b) evolution over time. The results were obtained by using the equivalent circuit and detailed parameters were reported in Table S2 in SI. The Nyquist plot showed that the semicircle expanded over time, indicating an increased charge transfer resistance. After 20 days, R_{ct} remained to be stable, which was confirmed in the Figure 3g. This resistance could be related to the formation of the passivation layer on the Li metal anode surface.[46,47] Whereas, R_b was very small and almost remained unchanged from the beginning. It is consistent with the previous report that the value of R_b will be very small when the conductivity of the SPE is above 0.1 mS/cm.[48] Based on the EIS data, a stable SPE with a passivation layer on the interface of Li metal anode were formed to prevent the electrolyte from further deterioration. This phenomenon suggested that the SPE is compatible with the Li metal anode for a safer operation in rechargeable Li metal batteries.

2.3 Lithium Metal Batteries with Solid Polymer Electrolyte

The contact between the porous electrode and the SPE is the key factor to determine the cell performance of SPE-based LMBs. To enhance the contact between the cathode and the SPE film, the cathode was coated with SPE precursor and then rested for overnight before the a free standing SPE film (250 -500 μm) was laminated and crosslinked. The cross-section SEM images of SPE with cathode are shown in Figure S5. The SEM shows the interface between the cathode and the SPE is smooth and flexible SPE is conformally coated on the porous cathode. 4 V cathode $LiNi_{0.8}Co_{0.15}Al_{0.05}O_2$ (NCA), which was recently used in state-of-art lithium ion batteries for electrical vehicle application,[8,49] replacing lithium iron phosphate (LFP), was used in this research. Most published solid polymer electrolytes work focused on LFP based cell due to the limited electrochemical window of the SPE.[50,51] To the best of our understanding, long cycling life of LMB with NCA cathode and SPE has not been demonstrated. The NCA based LMBs with the Li|SPE|NCA configuration were fabricated in this work and tested. The cells were first charged and discharged at an electrochemical window of 2.5 V to 3.9 V (*vs*. Li^+/Li) for initial cycles to achieve stable Coulombic efficiency, then the cells were cycled between 2.5 V to 4.15 V (*vs*. Li^+/Li) in the following cycles. Figure 4a demonstrates the capacities of NCA batteries at different current densities with 10 cycles per stage. The battery exhibited reversible specific capacities of about 156 mAh/g, 137 mAh/g, 116 mAh/g, 102 mAh/g, 89 mAh/g, 77 mAh/g, and 142 mAh/g at corresponding current density of 0.1 C, 0.2 C, 0.4 C, 0.6 C, 0.8 C, 1 C and 0.1 C (based on 1C=180 mAh/g). Figure 4b shows the corresponding charge/discharge profile in the ratability tests. Further long-term cycle performance testing was also conducted using the same NCA cells. The SPE based batteries were tested at 0.1 C for 500 cycles and 1 C for 1000 cycles. The cycling results are shown

in Figure 4c and 4d, respectively. The corresponding charge/discharge profiles were reported in Figure 4e and 4f. At 0.1 C (Figure 4c), the battery exhibited an initial specific capacity of ~ 165 mAh/g. The average Coulombic efficiency was over 99.78% for 500 cycles. The capacity retention after 100 cycles was 77% and the final retention was 48% after 500 cycles. At 1C (Figure 4d), the initial specific capacity of the cell was 113 mAh/g. The capacity retention after 100 cycles, 500 cycles and 1000 cycles were 77%, 72% and 66%, respectively. The average Coulombic efficiency was over 99.99% for 1000 cycles. It is worth mentioning that the capacity fading after the initial 100 cycles was very slow, with only 0.017%/cycle capacity fading in the rest of the 900 cycles. This indicates that the SPE based LMB is very stable once the initial passivation layer is successfully formed on the lithium metal anode. Additional tests for 0.2 C were also conducted (Figure S6a). The initial specific capacity was ~152 mAh/g with a ~45% retention on its 500th cycle. The average Coulombic efficiency of the battery was ~99.85%.

For comparison, the single salt (LiTFSI) SPE battery was tested as well (Figure S6c). As shown in SI, the capacity fading of the single salt SPE was very fast, with nearly no capacity remaining after just 100 cycles. This result is coherent with the previous reports, where single salt was applied in PEO, showing a rapid capacity fading at electrochemical window over 4 V.[52] Table S3 listed previous reports of the NCA cathode based LMB, including in solid-sate battery and liquid electrolyte-based cells. The dual-salt SPE LMBs reported in this work demonstrated similar long cycling stability as those liquid electrolyte-based batteries and are significantly better than previously reported solid state battery.[52-53] The results showed that the dual-salt SPE had the great potential to build up long cycling life LMBs with a high specific capacity 4 V cathode.

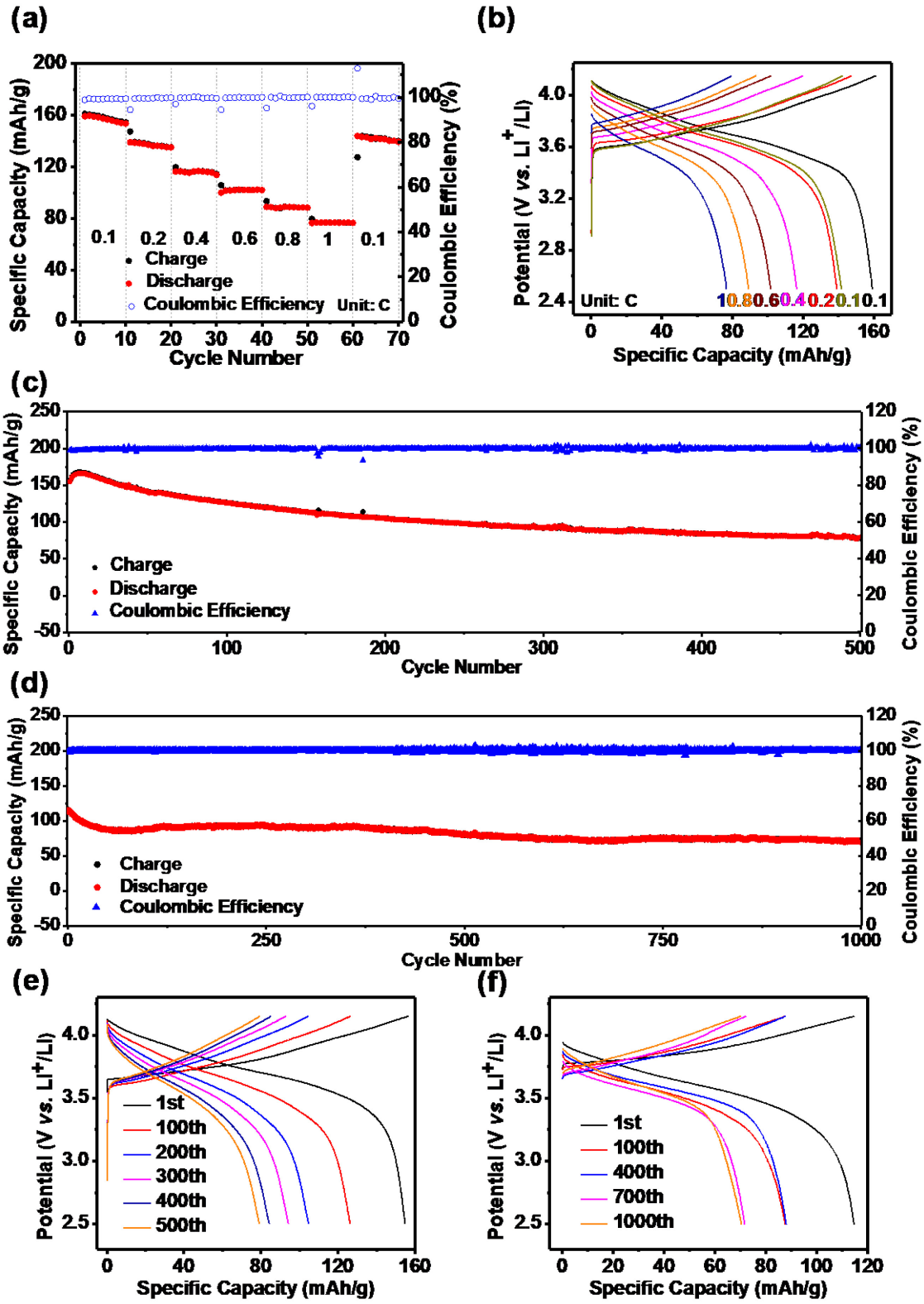
(a)
Specific Capacity (mAh/g)
Coulombic Efficiency (%)
Cycle Number
0.1 0.2 0.4 0.6 0.8 1 0.1
Charge
Discharge
Coulombic Efficiency
Unit: C
(b)
Potential (V vs. Li+/Li)
Specific Capacity (mAh/g)
Unit: C
1 0.8 0.6 0.4 0.2 0.1 0.1
(c)
Specific Capacity (mAh/g)
Coulombic Efficiency (%)
Cycle Number
Charge
Discharge
Coulombic Efficiency
(d)
Specific Capacity (mAh/g)
Coulombic Efficiency (%)
Cycle Number
Charge
Discharge
Coulombic Efficiency
(e)
Potential (V vs. Li+/Li)
Specific Capacity (mAh/g)
1st
100th
200th
300th
400th
500th
(f)
Potential (V vs. Li+/Li)
Specific Capacity (mAh/g)
1st
100th
400th
700th
1000th

Figure 4. (a) The rate performance of the SPE based LMB at 30 ºC from 0.1 C to 1 C as indicated. (b) The corresponding charge/discharge profiles of dual-salt SPE based LIB at different rates. (c) The long cycle performance of LMB at 0.1 C under 30 ºC. The initial activation cycles were operated in the range of 2.5 – 3.9 V at 0.1 C and not shown in all figures. The following cycles were operated from 2.5 V to 4.15 V at 0.1 C. (d) The long cycle performance of LMB at 1 C under 30 ºC. The initial activation cycles were operated in the range of 2.5 – 3.9 V at 0.1C and not shown in all figures. The following cycles were operated from 2.5 V to 4.15 V at 1 C. (e) The charge/discharge profiles of LMB at 0.1 C in 1^{st}, 100^{th}, 200^{th}, 300^{th}, 400^{th}, and 500^{th} cycles. (f) The charge/discharge profiles of LMB at 1 C in 1^{st}, 100^{th}, 400^{th}, 700^{th} and 1000^{th} cycles.

3. CONCLUSIONS

In conclusion, solid-state, highly conductive dual-salt polymer electrolyte were successfully designed and tested for lithium metal batteries with 4 V cathode. The free-standing SPE film was prepared by crosslinking the SPE precursor through UV-initiated polymerization. The ternary phase diagram analysis was used to guide the SPE design to reach the ideal ionic conductivity. The SPE with ionic conductivity over 1.76 mS/cm (at 30 ºC) was achieved. A dual-salt system (LiTFSI and LiBOB) was used to enhance the electrochemical stability of SPE. The system exhibited a wide electrochemical window of up to 4.8 V (*vs*. Li^+/Li) in LSV and CV and up to 4.15 V in lithium metal battery cells. The SPE was able to effectively suppress the lithium dendrite as indicated in the lithium plating/stripping tests at 30 ºC. The SPE film remained stable over 2300 hours with a current density of 0.1 mA/cm^2 and over 1700 hours at current density of 0.5 mA/cm^2. The dual-salt SPE based batteries delivered initial capacity of 165 mAh/g at 0.1 C and 113 mAh/g

at 1 C. The long cycle test of SPE based LMB at 1 C under 30 ºC exhibited outstanding stability with average Coulombic efficiency of over 99.99% and capacity retention over 77% after 100 cycles, 72% after 500 cycles and 66% after 1000 cycles. This work demonstrates a solid-state battery with a stable SPE system that can achieve high conductivity at room temperature, wide electrochemical window and long cycle stability with 4 V cathode.

Corresponding Author

* Yu Zhu. E-mail: yu.zhu@uakron.edu

Author Contributions All authors have given approval to the final version of the manuscript.

Conflict of Interest The authors declare the following competing financial interest(s): A provisional patent applications (USPTO 62/515,000) owned by University of Akron that disclose the high ionic conductivity solid polymer electrolyte composite.

Acknowledgments

The authors would like to thank Edwards Laughlin for the assistance in fabricating and designing the isothermal chamber. The authors thank the financial support from the National Science Foundation (NSF) through NSF-CBET 1505943, 1706681 and NSF-DMR 1554851.

Supporting Information Available Additional NMR, TGA, DSC and materials synthesis procedures. These materials are available free of charge *via* the Internet at http://pubs.acs.org.

REFERENCES

(1) Aurbach, D.; Zinigrad, E.; Cohen, Y.; Teller, H. A Short Review of Failure Mechanisms of Lithium Metal and Lithiated Graphite Anodes in Liquid Electrolyte Solutions. *Solid State Ionics* **2002**, *148*, 405–416.

(2) Wang, H.-G.; Yuan, S.; Ma, D.-L.; Zhang, X.-B.; Yan, J.-M. Electrospun Materials for Lithium and Sodium Rechargeable Batteries: From Structure Evolution to Electrochemical Performance. *Energy Environ. Sci.* **2015**, *8*, 1660–1681.

(3) Xu, K. Electrolytes and Interphases in Li-Ion Batteries and Beyond. *Chem. Rev.* **2014**, *114*, 11503–11618.

(4) Budde-Meiwes, H.; Drillkens, J.; Lunz, B.; Muennix, J.; Rothgang, S.; Kowal, J.; Sauer, D. U. A Review of Current Automotive Battery Technology and Future Prospects. *Proc. Inst. Mech. Eng. Part D J. Automob. Eng.* **2013**, *227*, 761–776.

(5) Bruce, P. G.; Freunberger, S. A.; Hardwick, L. J.; Tarascon, J.-M. Li-O2 and Li-S Batteries with High Energy Storage. *Nat. Mater.* **2012**, *11*, 19–29.

(6) Zhang, K.; Lee, G. H.; Park, M.; Li, W.; Kang, Y. M. Recent Developments of the Lithium Metal Anode for Rechargeable Non-Aqueous Batteries. *Adv. Energy Mater.* **2016**, *6*, 1–14.

(7) Kaskhedikar, N. A.; Maier, J. Lithium Storage in Carbon Nanostructures. *Adv. Mater.* **2009**, *21*, 2664–2680.

(8) Nitta, N.; Wu, F.; Lee, J. T.; Yushin, G. Li-Ion Battery Materials: Present and Future. *Mater. Today* **2015**, *18*, 252–264.

(9) He, Y.-B.; Li, B.; Liu, M.; Zhang, C.; Lv, W.; Yang, C.; Li, J.; Du, H.; Zhang, B.; Yang, Q.-

H. Gassing in Li4Ti5O12-Based Batteries and Its Remedy. *Sci. Rep.* **2012**, *2*, 913.

(10) Teshima, K.; Inagaki, H.; Tanaka, S.; Yubuta, K.; Hozumi, M.; Kohama, K.; Shishido, T.; Oishi, S. Growth of Well-Developed Li4Ti5O12 Crystals by the Cooling of a Sodium Chloride Flux. *Cryst. Growth Des.* **2011**, *11*, 4401–4405.

(11) Thackeray, M. M.; Kang, S.-H.; Johnson, C. S.; Vaughey, J. T.; Benedek, R.; Hackney, S. A. Li 2 MnO 3-Stabilized LiMO 2 (M= Mn, Ni, Co) Electrodes for Lithium-Ion Batteries. *J. Mater. Chem.* **2007**, *17*, 3112–3125.

(12) Yoshio, M.; Wang, H.; Fukuda, K.; Umeno, T.; Dimov, N.; Ogumi, Z. Carbon-Coated Si as a Lithium-Ion Battery Anode Material. *J. Electrochem. Soc.* **2002**, *149*, A1598–A1603.

(13) Slater, M. D.; Kim, D.; Lee, E.; Johnson, C. S. Sodium-ion Batteries. *Adv. Funct. Mater.* **2013**, *23*, 947–958.

(14) Cao, C.; Li, Z.-B.; Wang, X.-L.; Zhao, X.-B.; Han, W.-Q. Recent Advances in Inorganic Solid Electrolytes for Lithium Batteries. *Front. Energy Res.* **2014**, *2*, 25.

(15) Lin, D.; Liu, Y.; Cui, Y. Reviving the Lithium Metal Anode for High-Energy Batteries. *Nat. Nanotechnol.* **2017**, *12*, 194–206.

(16) Dias, F. B.; Plomp, L.; Veldhuis, J. B. J. Trends in Polymer Electrolytes for Secondary Lithium Batteries. *J. Power Sources* **2000**, *88*, 169–191.

(17) Zhamu, A.; Chen, G.; Liu, C.; Neff, D.; Fang, Q.; Yu, Z.; Xiong, W.; Wang, Y.; Wang, X.; Jang, B. Z. Reviving Rechargeable Lithium Metal Batteries: Enabling next-Generation High-Energy and High-Power Cells. *Energy Environ. Sci.* **2012**, *5*, 5701–5707.

(18) Cheng, X.; Zhang, R.; Zhao, C.; Wei, F.; Zhang, J.; Zhang, Q. A Review of Solid Electrolyte

Interphases on Lithium Metal Anode. *Adv. Sci.* **2016**, *3*, 1500215.

(19) Wild, M.; O'Neill, L.; Zhang, T.; Purkayastha, R.; Minton, G.; Marinescu, M.; Offer, G. J. Lithium Sulfur Batteries, a Mechanistic Review. *Energy Environ. Sci.* **2015**, *8*, 3477–3494.

(20) Geng, D.; Ding, N.; Hor, T. S.; Chien, S. W.; Liu, Z.; Wuu, D.; Sun, X.; Zong, Y. From Lithium-Oxygen to Lithium-Air Batteries: Challenges and Opportunities. *Adv. Energy Mater.* **2016**, *6*, 1502164.

(21) Monroe, C.; Newman, J. The Impact of Elastic Deformation on Deposition Kinetics at Lithium/Polymer Interfaces. *J. Electrochem. Soc.* **2005**, *152*, A396–A404.

(22) Armand, M. B.; Chabagno, J. M.; Duclot, M. J. Fast Ion Transport in Solids. *Eds. Vashishta, P., Mundy, JN Shenoy, G. K, North Holland, Amsterdan* **1979**, *52*.

(23) Wright, P. V. Electrical Conductivity in Ionic Complexes of Poly (Ethylene Oxide). *Polym. Int.* **1975**, *7*, 319–327.

(24) Smitha, B.; Sridhar, S.; Khan, A. A. Solid Polymer Electrolyte Membranes for Fuel Cell Applications-a Review. *J. Memb. Sci.* **2005**, *259*, 10–26.

(25) Kuo, P.-L.; Wu, C.-A.; Lu, C.-Y.; Tsao, C.-H.; Hsu, C.-H.; Hou, S.-S. High Performance of Transferring Lithium Ion for Polyacrylonitrile-Interpenetrating Crosslinked Polyoxyethylene Network as Gel Polymer Electrolyte. *ACS Appl. Mater. Interfaces* **2014**, *6*, 3156–3162.

(26) Deng, F.; Wang, X.; He, D.; Hu, J.; Gong, C.; Ye, Y. S.; Xie, X.; Xue, Z. Microporous Polymer Electrolyte Based on PVDF/PEO Star Polymer Blends for Lithium Ion Batteries. *J. Memb. Sci.* **2015**, *491*, 82–89.

(27) Shi, J.; Yang, Y.; Shao, H. Co-Polymerization and Blending Based PEO/PMMA/P (VDF-HFP) Gel Polymer Electrolyte for Rechargeable Lithium Metal Batteries. *J. Memb. Sci.* **2018**, *547*, 1–10.

(28) Karan, N. K.; Pradhan, D. K.; Thomas, R.; Natesan, B.; Katiyar, R. S. Solid Polymer Electrolytes Based on Polyethylene Oxide and Lithium Trifluoro-Methane Sulfonate (PEO–LiCF3SO3): Ionic Conductivity and Dielectric Relaxation. *Solid State Ionics* **2008**, *179*, 689–696.

(29) Gorecki, W.; Jeannin, M.; Belorizky, E.; Roux, C.; Armand, M. Physical Properties of Solid Polymer Electrolyte PEO (LiTFSI) Complexes. *J. Phys. Condens. Matter* **1995**, *7*, 6823.

(30) Evans, J.; Vincent, C. A.; Bruce, P. G. Electrochemical Measurement of Transference Numbers in Polymer Electrolytes. *Polymer (Guildf).* **1987**, *28*, 2324–2328.

(31) Ghosh, A.; Wang, C.; Kofinas, P. Block Copolymer Solid Battery Electrolyte with High Li-Ion Transference Number. *J. Electrochem. Soc.* **2010**, *157*, A846–A849.

(32) Rietman, E. A.; Kaplan, M. L.; Cava, R. J. Lithium Ion-Poly (Ethylene Oxide) Complexes. I. Effect of Anion on Conductivity. *Solid State Ionics* **1985**, *17*, 67–73.

(33) Qian, X.; Gu, N.; Cheng, Z.; Yang, X.; Wang, E.; Dong, S. Plasticizer Effect on the Ionic Conductivity of PEO-Based Polymer Electrolyte. *Mater. Chem. Phys.* **2002**, *74*, 98–103.

(34) He, R.; Kyu, T. Effect of Plasticization on Ionic Conductivity Enhancement in Relation to Glass Transition Temperature of Crosslinked Polymer Electrolyte Membranes. *Macromolecules* **2016**, *49*, 5637–5648.

(35) Echeverri, M.; Hamad, C.; Kyu, T. Highly Conductive, Completely Amorphous Polymer

Electrolyte Membranes Fabricated through Photo-Polymerization of Poly (Ethylene Glycol Diacrylate) in Mixtures of Solid Plasticizer and Lithium Salt. *Solid State Ionics* **2014**, *254*, 92–100.

(36) Meyer, W. H. Polymer Electrolytes for Lithium-Ion Batteries. *Adv. Mater.* **1998**, *10*, 439–448.

(37) Chen, R.; Qu, W.; Guo, X.; Li, L.; Wu, F. The Pursuit of Solid-State Electrolytes for Lithium Batteries: From Comprehensive Insight to Emerging Horizons. *Mater. Horiz.* **2016**, *3*, 487–516.

(38) Mao, G.; Perea, R. F.; Howells, W. S.; Price, D. L.; Saboungi, M.-L. Relaxation in Polymer Electrolytes on the Nanosecond Timescale. *Nature* **2000**, *405*, 163.

(39) Do, C.; Lunkenheimer, P.; Diddens, D.; Götz, M.; Weiß, M.; Loidl, A.; Sun, X.-G.; Allgaier, J.; Ohl, M. Li+ Transport in Poly (Ethylene Oxide) Based Electrolytes: Neutron Scattering, Dielectric Spectroscopy, and Molecular Dynamics Simulations. *Phys. Rev. Lett.* **2013**, *111*, 18301.

(40) Quartarone, E.; Mustarelli, P. Electrolytes for Solid-State Lithium Rechargeable Batteries: Recent Advances and Perspectives. *Chem. Soc. Rev.* **2011**, *40*, 2525–2540.

(41) Zhang, J.; Huang, X.; Wei, H.; Fu, J.; Liu, W.; Tang, X. Preparation and Electrochemical Behaviors of Composite Solid Polymer Electrolytes Based on Polyethylene Oxide with Active Inorganic–organic Hybrid Polyphosphazene Nanotubes as Fillers. *New J. Chem.* **2011**, *35*, 614–621.

(42) Zugmann, S.; Fleischmann, M.; Amereller, M.; Gschwind, R. M.; Wiemhöfer, H. D.; Gores,

H. J. Measurement of Transference Numbers for Lithium Ion Electrolytes via Four Different Methods, a Comparative Study. *Electrochim. Acta* **2011**, *56*, 3926–3933.

(43) Ehrl, A.; Landesfeind, J.; Wall, W. A.; Gasteiger, H. A. Determination of Transport Parameters in Liquid Binary Lithium Ion Battery Electrolytes I. Diffusion Coefficient. *J. Electrochem. Soc.* **2017**, *164*, A826–A836.

(44) Nayak, P. K.; Grinblat, J.; Levi, M.; Aurbach, D. Understanding the Effect of Lithium bis(oxalato) Borate (LiBOB) on the Structural and Electrochemical Aging of Li and Mn Rich High Capacity Li1.2Ni0.16Mn0.56Co0.08O2 Cathodes. *J. Electrochem. Soc.* **2015**, *162*, A596–A602.

(45) Li, S.; Chen, Y.-M.; Liang, W. F.; Shao, Y. F.; Liu, K. W.; Nikolov, Z.; Zhu, Y. A Superionic Conductive, Electrochemically Stable Dual-Salt Polymer Electrolyte. *Joule* **2018**, 2, 1–19.

(46) Appetecchi, G.; Croce, F.; Persi, L.; Ronci, F.; Scrosati, B. Transport and Interfacial Properties of Composite Polymer Electrolytes. *Electrochim. Acta* **2000**, *45*, 1481–1490.

(47) Croce, F.; Curini, R.; Martinelli, A.; Persi, L.; Ronci, F.; Scrosati, B.; Caminiti, R. Physical and Chemical Properties of Nanocomposite Polymer Electrolytes. *J. Phys. Chem. B* **1999**, *103*, 10632–10638.

(48) Borghini, M. C.; Mastragostino, M.; Zanelli, A. Reliability of Lithium Batteries with Crosslinked Polymer Electrolytes. *Efecrrochwnico Am* **1996**, *41*, 2369–2373.

(49) Martha, S. K.; Haik, O.; Zinigrad, E.; Exnar, I.; Drezen, T.; Miners, J. H.; Aurbach, D. On the Thermal Stability of Olivine Cathode Materials for Lithium-Ion Batteries. *J. Electrochem. Soc.* **2011**, *158*, A1115–A1122.

(50) Nair, J. R.; Porcarelli, L.; Bella, F.; Gerbaldi, C. Newly Elaborated Multipurpose Polymer Electrolyte Encompassing RTILs for Smart Energy-Efficient Devices. *ACS Appl. Mater. Interfaces* **2015**, *7*, 12961–12971.

(51) Chen, B.; Xu, Q.; Huang, Z.; Zhao, Y.; Chen, S.; Xu, X. One-Pot Preparation of New Copolymer Electrolytes with Tunable Network Structure for All-Solid-State Lithium Battery. *J. Power Sources* **2016**, *331*, 322–331.

(52) Wetjen, M.; Kim, G.-T.; Joost, M.; Appetecchi, G. B.; Winter, M.; Passerini, S. Thermal and Electrochemical Properties of PEO-LiTFSI-Pyr14TFSI-Based Composite Cathodes, Incorporating 4 V-Class Cathode Active Materials. *J. Power Sources* **2014**, *246*, 846–857.

(53) Ito, S.; Fujiki, S.; Yamada, T.; Aihara, Y.; Park, Y.; Kim, T. Y.; Baek, S.-W.; Lee, J.-M.; Doo, S.; Machida, N. A Rocking Chair Type All-Solid-State Lithium Ion Battery Adopting Li_2O–ZrO_2 Coated $LiNi_{0.8}Co_{0.15}Al_{0.05}O_2$ and a Sulfide Based Electrolyte. *J. Power Sources* **2014**, *248*, 943-950.

TOC

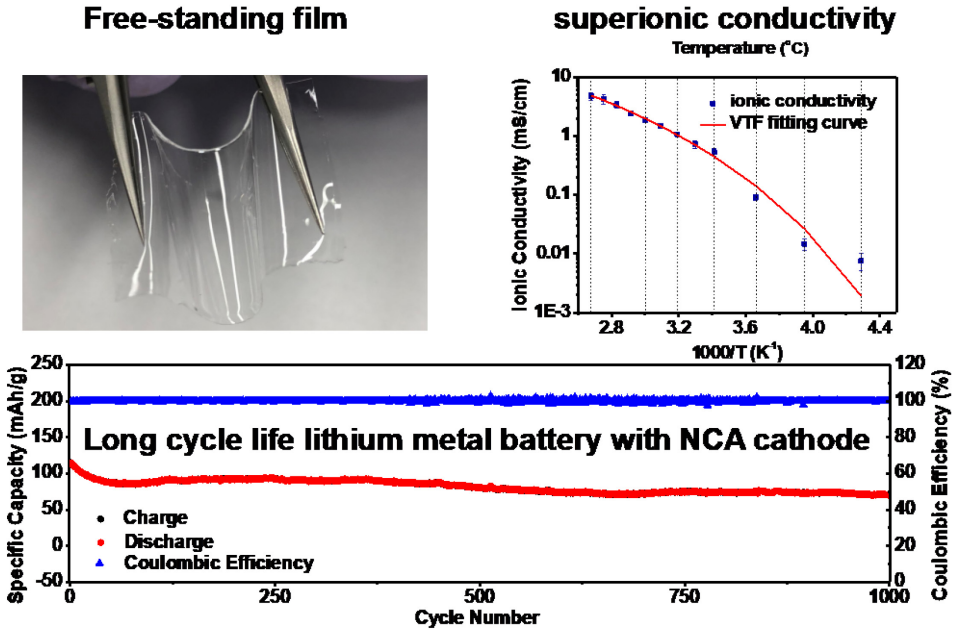
Free-standing film
superionic conductivity
Temperature (°C)
Ionic Conductivity (mS/cm)
ionic conductivity
VTF fitting curve
1000/T (K-1)
Long cycle life lithium metal battery with NCA cathode
Charge
Discharge
Coulombic Efficiency
Specific Capacity (mAh/g)
Coulombic Efficiency (%)
Cycle Number